

Photonic crystal nanocavity array laser

Hatice Altug and Jelena Vučković

Edward L. Ginzton Laboratory, Stanford University, Stanford, CA, 94305-4088

altug@stanford.edu

Abstract: We demonstrate a new type of laser composed of an array of coupled photonic crystal nanocavities that enables high differential quantum efficiency and output power, together with a low threshold power comparable to those of single photonic crystal cavity lasers. In our experiment, the laser efficiency increases faster than the lasing threshold with an increase in the number of coupled cavities. We observe a single mode lasing and measure the output powers that are two orders of magnitude higher than in single nanocavity lasers. Finally, we study the laser behavior theoretically and show that the benefits resulting from the coupling of cavities are due to strong cavity effects such as the enhanced spontaneous emission rate.

© 2005 Optical Society of America

OCIS codes: (140.3460) Lasers; (140.3290) Laser arrays; (140.3570) single-mode Lasers; (140.3410) Laser resonators; (140.4780) Optical resonators; (230.3990) Microstructure devices; (250.5300) Photonic integrated circuits; (260.5740) Resonance; (270.3430) Laser theory; (130.3120) Integrated optics devices

References and Links

1. J.L. Jewell, J. P. Harbison, A. Scherer, Y.H. Lee, and L.T. Florez, "Vertical-cavity surface emitting lasers: Design, growth, fabrication, characterization," *IEEE J. Quantum Electron.* **27**, 1332-1346 (1991)
2. K. L. Lear, et. al. "Small and large signal modulation of 850 nm oxide-confined vertical cavity surface emitting lasers", *Advances in Vertical Cavity Surface Emitting Lasers in series OSA Trends in Optics and Photonics* **15**, 69-74 (1997)
3. E.Yablonovitch, "Inhibited Spontaneous Emission in Solid-State Physics and Electronics," *Phys. Rev. Lett.* **58**, 2059-2062 (1987)
4. S. John, "Strong localization of photons in certain disordered dielectric superlattices," *Phys. Rev. Lett.* **58**, 2486-2489 (1987)
5. Purcell, "Spontaneous emission Probabilities at Radio Frequencies," *Phys. Rev.* **69**, 681 (1946)
6. O. Painter, R.K. Lee, A. Scherer, A. Yariv, J. D. O'Brien, P.D. Dapkus, and I. Kim, "Two-Dimensional Photonic Band-Gap Defect Mode Laser," *Science* **284**, 1819-1821 (1999)
7. M. Loncar, T. Yoshie, A. Scherer, P. Gogna, and Y. Qiu, "Low-threshold photonic crystal laser," *Appl. Phys. Lett.* **81**, 2680-2682 (2002)
8. H. G. Park, S.H. Kim, S.H. Kwon, Y.G. Ju, J.K. Yang, J.H. Baek, S.B. Kim, and Y.H. Lee, "Electrically Driven Single-Cell Photonic Crystal Laser," *Science* **305**, 1444-1447 (2004)
9. T. Yoshie, M. Loncar, A. Scherer, and Y. Qiu, "High Frequency Oscillation in Photonic Crystal nanolasers," *Appl. Phys. Lett.* **84**, 3543-3545 (2004)
10. M. Meier, A. Mekis, A. Dobabalapur, A. Timko, R. E. Slusher, J. D. Joannopoulos, and O. Nalamasu, "Laser action from two-dimensional distributed feedback in photonic crystals," *Appl. Phys. Lett.* **74**, 7-9, (1999)
11. S. Noda, M. Yokoyama, M. Imada, A. Chutinan, and M. Mochizuki, "Polarization Mode Control of Two-Dimensional Photonic Crystal Laser by Unit Cell Structure Design," *Science* **293**, 1123-1125 (2001)
12. C. Monat, C. Seassal, X. Letartre, et. al. "InP-based two-dimensional photonic crystal on silicon: In-plane Bloch mode laser," *Appl. Phys. Lett.* **81**, 5102-5104 (2002)
13. M. Imada, S. Noda, A. Chutinan, and T. Tokuda, "Coherent two-dimensional lasing action in surface-emitting laser with triangular-lattice photonic crystal structure," *Appl. Phys. Lett.* **75**, 316-318 (1999)
14. H. Altug, and J. Vuckovic, "Two-dimensional coupled photonic crystal resonator arrays," *Appl. Phys. Lett.* **84**, 161-163 (2004)
15. D. G. Deppe, J. P. van der Ziel, N. Chand, G. J. Zydzik, and S. N. G. Chu, "Phase-coupled two-dimensional $\text{Al}_x\text{Ga}_{1-x}\text{As}$ -GaAs vertical-cavity surface-emitting laser array," *Appl. Phys. Lett.* **56**, 2089-2091 (1990)

16. M. Orenstein, E. Kapon, N. G. Stoofel, J. P. Harbison, J. Wullert, "Two-dimensional phase-locked arrays of vertical-cavity semiconductor lasers by mirror reflectivity modulation," *Appl. Phys. Lett.* **58**, 804-806 (1991)
17. M. E. Warren, P.L. Gourley, G. R. Hadley, G. A Vawter, T. M. Brennan, B. E. Hammons, K. L. Lear, "On-axis far-field emission from two-dimensional phase-locked vertical cavity surface-emitting laser arrays with an integrated phase-corrector," *Appl. Phys. Lett.*, **61**, 1484-1486 (1992)
18. J. J. Raftery, A.J. Danner, J. C. Lee, K. D. Choquette, "Coherent coupling of two-dimensional arrays of defect cavities in photonic crystal vertical cavity surface-emitting lasers," *Appl. Phys. Lett.* **86**, 201104- (2005)
19. H. Altug, J. Vuckovic, "Experimental demonstration of the slow group velocity of light in two-dimensional coupled photonic crystal microcavity arrays," *Appl. Phys. Lett.* **86**, 111102 (2005)
20. H. Altug, J. Vuckovic, "Polarization control and sensing with two-dimensional coupled photonic crystal microcavity arrays," *Optics Lett.* **30**, 982-984 (2005)
21. A. Imamoglu, Y. Yamamoto, *Mesoscopic Quantum Optics*, New York: Wiley, 1999
22. L. A. Coldren, S. W. Corzine, *Diode Lasers and Photonic Integrated Circuits*, New York: Wiley, 1995
23. A. Xing, M. Davanco, D. J. Blumenthal, E. Hu, "Fabrication of InP-based photonic crystal membrane," *J. Vacuum Science B*, **22** 70-73 (2004)
24. J.R. Cao, P.T. Lee, S.J. Choi, R. Shafiiha, S.J. Choi, J. D. O'Brien, P. D. Dapkus, "Nanofabrication of photonic crystal membrane lasers," *J. Vacuum Science B*, **20**, 618-621 (2002)
25. T. Baba, "Photonic crystals and microdisk cavities based on GaInAsP-InP system," *IEEE J. Select. Topics Quantum Electron.*, **3**, 808-811 (1997)
26. T. D. Happ, M. Kamp, A. Forchel, J. Gentner, L. Goldstein, "Two-dimensiona photonic crystal coupled-defect laser diode," *App. Phys. Lett.* **82**, 4 (2003)
27. A. Nakagawa, S. Ishii, T. Baba, "Photonic molecule laser composed of GaInAsP microdisks," *Appl. Phys. Lett.* **86**, 041112 (2005)

1. Introduction

A single mode laser that can be turned on at low pump powers, directly modulated at high speeds and that can produce sufficiently high output powers is crucial for applications ranging from optical telecommunications and optical interconnects, to spectroscopic sensing and optical image processing. Vertical cavity surface emitting lasers (VCSELs), first demonstrated in 1989 [1], have been investigated extensively as promising candidates for these purposes; however they suffer from limitations such as relatively high threshold powers, multi-mode operation, problems with direct modulation above 20GHz [2], and difficulty in growing their Distributed Bragg Reflectors for long-haul telecommunications wavelengths.

In recent years, high quality factor, small-mode volume cavities based on photonic crystals (PCs) [3-4] have attracted significant attention, because of their ability to modify the density of optical states (DOS) strongly. An increase in DOS of the lasing mode causes significant enhancement of the spontaneous emission rate (Purcell effect) [5]. This consequently enables larger fractions of photons to be emitted into the lasing mode with respect to all other modes (denoted as spontaneous emission-coupling factor β) and reduces the lasing threshold [6-8]. The β -factor in VCSELs is typically less than 10^{-3} , but it can be increased by two orders of magnitude in photonic crystal nanocavities. In addition, the Purcell effect also increases the achievable direct modulation speed [9]. Unfortunately, output power levels of such PC nanocavity lasers are extremely low (a few nW), below the levels needed for many practical applications. In an attempt to increase output powers of PC lasers, band-edge lasers have been investigated recently [10-12]. However, they do not offer the aforementioned benefits of nanocavity lasers, and can also suffer from multimode lasing [13].

To overcome these problems, we recently proposed two-dimensional coupled PC nanocavity array lasers [14]. In this paper, we describe the experimental demonstration of such a laser, which operates in a single mode and produces output powers that are two orders of magnitude higher than those of single nanocavity lasers. We also show that the laser efficiency increases faster than the lasing threshold with an increase in the number of coupled cavities. We note that the coupling of a small number of VCSELs has been previously investigated [15-18]. However, it is very hard to control the uniformity of the arrays and the

coupling between individual lasers, which are necessary to achieve the phase-locked lasing from a large number of cavities. Moreover, a rather complicated fabrication procedure has been used to achieve phase-locked lasing even from small number of coupled cavity arrays [17]. With photonic crystal nanocavity arrays, we can control both the uniformity and the coupling very precisely (e.g., we have recently demonstrated arrays consisting of 3600-coupled PC nanocavities in silicon [19-20]). In our laser, each cavity forming the array occupies an area of only $1.5\mu\text{m}^2$ (much smaller than a typical VCSEL), implying that an ultra-dense packing is achievable with coupled PC nanocavities lasers, which can also enable higher output powers. Finally, we study the behavior of our laser theoretically and show that the full benefits resulting from the coupling of cavities are achievable only if strong cavity effects are present (i.e., large β factor), implying that the coupling of PC nanocavities is preferential over coupling of larger resonators (e.g., VCSELs).

2. Theoretical analysis of a nanocavity array laser

As described above, we show here that the full benefits of the cavity array lasers are achievable only when the cavity effects are strong (i.e. large β), as it is in our PC nanocavity arrays. The threshold pump power ($L_{\text{in,th}}$) is defined as the input pump power at which the photon number inside the optical mode volume is equal to 1 [21] and the differential quantum efficiency (DQE) is defined as the slope of the laser output-input power curve (LL-curve) above threshold [22]. Starting with the rate equations in the steady-state (see Appendix) and assuming that the carrier density and the gain above threshold are clamped to their values at the threshold [22], and that the nonradiative decay rate is much slower than radiative rate, one can derive an expression for $L_{\text{in,th}}$ and DQE:

$$L_{\text{in,th}} = \frac{\hbar\omega_p V_a}{\eta} \left[\frac{1}{\tau_p V_{\text{mode}}} - \beta \frac{N_{\text{th}}}{\tau_r} + \frac{N_{\text{th}}}{\tau_r} \right] \quad (1)$$

$$\text{DQE} = \eta \frac{\omega_l}{\omega_p} \frac{V_{\text{mode}}}{V_a} \frac{1}{\tau_{\text{mirror}}} \frac{1}{\Gamma G(N_{\text{th}})} \quad (2)$$

In this derivation, in contrary to the usual assumption of neglecting the β term [22], we keep it since it is significant in nanocavities studied here. In the expressions above, ω_p is the pump laser frequency, ω_l the laser emission frequency, η the absorption ratio of the pump in the active region, V_a the pumped active volume, V_{mode} the optical mode volume, $\tau_p = Q/\omega_l$ is the photon lifetime (Q is the quality factor of the optical mode), τ_r the carrier radiative lifetime, N_{th} the carrier density at threshold, $1/\tau_{\text{mirror}}$ the photon loss rate towards detection system (ideally $\tau_{\text{mirror}} = \tau_p$, if all emitted photons are collected), Γ the confinement factor, and $G(N_{\text{th}})$ the gain at the threshold. From the rate equations, the gain at threshold can be expressed as:

$$\Gamma G(N_{\text{th}}) = \frac{1}{\tau_p} - \beta \frac{N_{\text{th}} V_{\text{mode}}}{\tau_r} \quad (3)$$

When n_c individual lasers are coupled in an array, both V_{mode} and V_a increase by a factor roughly equal to n_c (relative to a single laser). In addition, the photon storage time τ_p (and consequently τ_{mirror}) can increase (by n_c times for ideal 3-D coupled nanocavity arrays). Hence, for non-negligible β , $\tau_{\text{mirror}} \Gamma G(N_{\text{th}})$ decreases in a coupled laser array which leads to an increase in DQE. In an ideal case ($\beta \approx 1$), according to (1)-(3), coupled cavity lasers would have the same threshold as single cavity lasers since the 2nd and 3rd term in (1) cancel each

other and $L_{in,th}$ becomes independent of n_c , but with a much higher DQE. On the other hand, if β is negligible and V_{mode} is large (as it is in VCSELs), $L_{in,th}$ of the laser array increases roughly n_c times relative to an individual laser (as the 3rd term in (1) dominates), while DQE does not change (as the threshold gain is primarily determined by $1/\tau_p$ in (3)). PC nanocavity arrays that are shown here are somewhere in between these two extreme cases: their β is non-negligible and V_{mode} is small, implying that different terms in the expression for $L_{in,th}$ and $G(N_{th})$ become comparable. Therefore, DQE of the PC cavity array lasers increases relative to that of a single PC cavity laser, while the increase in the lasing threshold is slower than the increase in the number of cavities.

It should also be pointed out that in PC nanocavity array lasers, V_a increases slower than V_{mode} with an increase in the number of cavities. Hence, the ratio V_{mode}/V_a is larger for nanocavity array laser than for a single PC cavity laser, leading to an additional increase in DQE, which we observe in our experiment below. This effect is a result of a more efficient pumping and the better overlap between the pumped area and the cavity mode. In a single PC cavity laser, it is extremely difficult to pump only the central cavity region, and the pump also generates carriers inside the mirrors, which do not couple to the lasing mode. On the other hand, in a coupled array laser one can pack larger number of lasers more efficiently by reducing the space used as mirrors, and the overlap between the pumped region and the cavity mode is better.

3. Experimental results

3.1. Design and fabrication of the laser structure

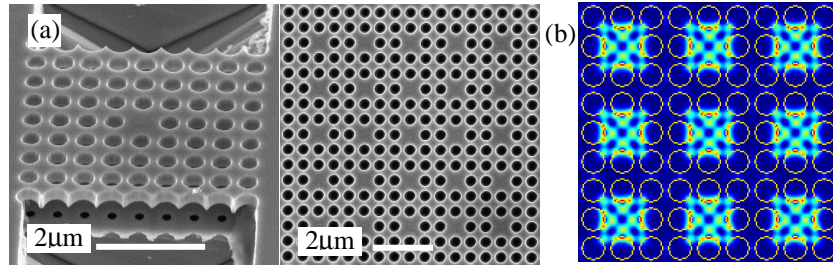


Fig. 1. (a) SEM pictures of a fabricated single PC cavity laser and a coupled PC cavity array laser (b) Simulated electric field amplitude of the coupled cavity array quadrupole mode at the Γ -point in the middle of the slab.

Here, we focus on arrays of nanocavities in a square lattice PC and choose non-degenerate high Q- factor (~ 2000) quadrupole mode (field pattern is shown in Fig. 1(b) [14,19]. We fabricated such nanocavity arrays in InP material system. The active region contains four InGaAsP quantum wells (QWs) with a peak photoluminescence emission wavelength of 1560nm (Fig.2). Fabrication process starts with the PECVD deposition of 90 nm thick SiO_2 followed by spinning of the 380 nm thick PMMA layer. Electron-beam lithography is used to define the patterns in PMMA. First, the patterns are transferred from PMMA layer to oxide mask using reactive ion etch with CHF_3/O_2 gas combination and then transferred from oxide mask to InGaAsP slab layer using $\text{Cl}_2/\text{Ar}/\text{BCl}_3$ gas combination at 200°C. Finally the InP sacrificial layer under the slab is released by immersing the sample into $\text{HCl}:\text{H}_2\text{O}$ (4:1). During the lithography step trenches are opened at the sides of the structure (Fig. 1) to ease the undercut of sacrificial layer [23,24]. The coupled array consists of 81 cavities (9x9) with two layers of photonic crystal in between. PC parameters are the free-standing membrane thickness (d) of 280nm, periodicity (a) of 500nm, and the hole radius (r) tuned from 160nm to 230nm to change the resonance frequency of cavities. Single cavity lasers are also fabricated

on the same chip, with the same parameter range. With these parameters, the quadrupole mode frequency calculated by the Finite Difference Time Domain (FDTD) method falls within the gain linewidth.

3.2. Experimental set-up

The coupled PC nanocavity array lasers with sizes $\sim 15\mu\text{m}$ are optically pulse-pumped normal to the structure at room temperature. A diode laser at 808nm is focused on the sample with a spot size of $\sim 15\mu\text{m}$ by a 40x microscope objective lens with a numerical aperture of 0.6. The pump pulses are 20ns long with 1% duty cycle, chosen to reduce the heating of the structure. Emitted light is collected from the top of the sample (in the Γ direction, perpendicular to the sample surface) using the same optics and coupled to an optical spectrum analyzer. To compare the performance of the coupled cavity array lasers to that of single nanocavity lasers (with size $\sim 4\mu\text{m}$), a similar setup with a beam spot size of $\sim 5\mu\text{m}$ is used.

3.3. Coupled PC nanocavity array laser spectrum

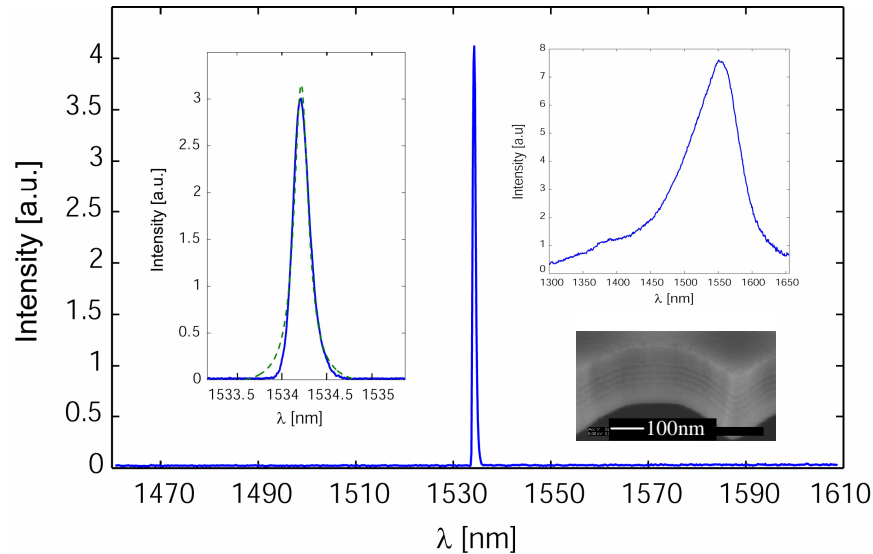


Fig. 2. (a) Spectrum of the coupled cavity array laser with a peak at 1534nm. The PC hole radius in this structure is about 192nm. The inset on the left shows the zoomed-in portion of the spectrum fitted with a Lorentzian (green dashed curve) of 0.23nm linewidth. The inset on the right shows the QW photoluminescence from unprocessed wafer (QWs shown on the SEM image).

Single mode lasing is observed from coupled nanocavity array lasers (spectrum is shown in Fig. 2). The lasing wavelength matches that of the phase-coupled quadrupole mode at the Γ -point calculated by FDTD. The collection angle of the objective lens is wide enough to collect the emission from any other possible modes [14]. However, we observe only a single mode in the spectrum, even at low powers. A slight linewidth narrowing was observed above threshold, while the spectrum below the threshold was hard to measure due to the poor sensitivity of spectrum analyzer.

3.4. Lasing mode imaged on the IR-camera

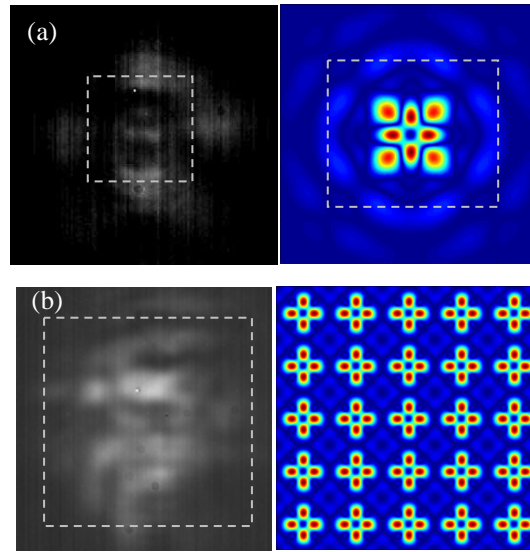


Fig. 3. (a) The IR-camera image (left) and the simulated time-averaged Poynting vector in the vertical direction (right) of the lasing mode for a single cavity laser. The size of the structure is indicated by the dashed square. (b) The same for a coupled cavity array laser.

The profiles of the lasing modes both from a single cavity and a coupled cavity array laser taken with an infrared-camera are shown in Fig. 3. The setup used for probing a single cavity has a higher magnification and shows clearly the four-fold symmetry of the mode, which is expected for the quadrupole. At the center of the square, there is a strong field localization, corresponding to the location of the single defect. A strong radiation leak outside the square is also visible, which is due to the fact that the cavity is surrounded by only four PC layers. The set-up used for probing coupled cavity array laser has a lower magnification, and therefore individual cavities are hard to resolve, but emission from most of the array is visible. The radiation profiles for the quadrupole mode are simulated by the FDTD method, by calculating the time averaged Poynting vector in the vertical direction. The radiation patterns corresponding to the plane positioned at $\sim 1\mu\text{m}$ above the structure are very similar to the experimentally measured field patterns, as shown in Fig. 3. The match is especially good for a single cavity, where both localized and leaking field components are nicely reproduced in the simulation.

3.5. LL curve

Coupled nanocavity array lasers with different r/a ratios have been tested and Fig. 4 shows the measured light-out/light-in (LL) curve of one of them (blue). We have observed single-mode lasing at 1534nm with a threshold peak pump power of $\sim 2.4\text{mW}$. Several single cavity structures with different r/a have also been tested. The LL-curve of one of them (with $r/a \approx 0.4$) is shown in Fig. 4 (red). The parameters of this cavity and therefore the emission wavelength at 1543nm are quite similar to the coupled cavity array laser, giving an additional indication that the quadrupole mode and the phase-coupled quadrupole band at the Γ point are the lasing modes for a single cavity laser and a couple nanocavity array laser, respectively. The threshold peak pump power is around $\sim 320\mu\text{W}$.

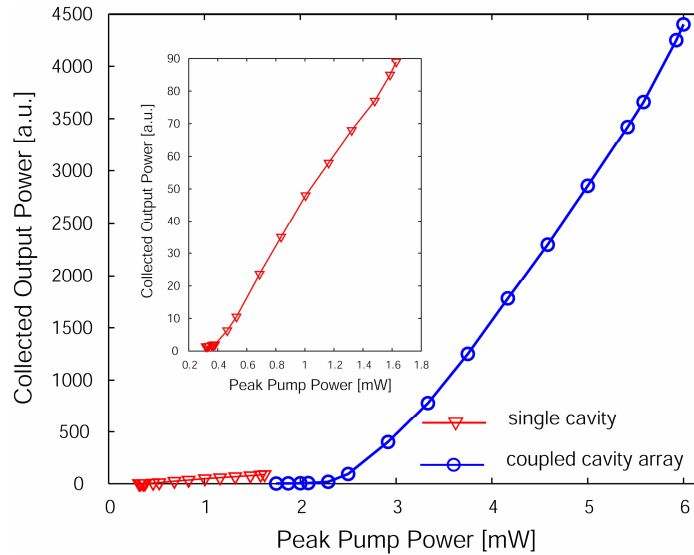


Fig. 4. LL-curves of the single PC cavity and the coupled PC cavity array laser. The inset shows a magnified curve for the single PC cavity

By fitting laser rate equations with the typical InGaAsP QW parameters (listed in Table 2 in appendix) to the LL-curves of both lasers we obtain the range of β values given in Table 1 [5, 22, 25]. β of the coupled cavity array laser is estimated to be slightly smaller than β of a single cavity, but it is still large enough to observe strong cavity effects mentioned above. We have measured the threshold peak power and DQE of the LL-curve for several different coupled array and single nanocavity lasers; the averaged results are given in Table 1. The measured lasing threshold of coupled photonic crystal nanocavity arrays is about 10 times larger than for a single cavity. According to the parameters that we use in the β -fit, the third term in (1) dominates the threshold expression, so we expect that the threshold pump power scales with the pumped active volume V_a . In the experiment, the size of the pump beam size for coupled cavity laser is almost 10 times larger than for a single cavity laser, which explains the observed increase in threshold. On the other hand, the measured 20-fold increase in DQE of the cavity array is larger than the increase in threshold, implying that a higher output power can be extracted per nanocavity in a coupled cavity array laser in comparison to a single nanocavity laser. In fact, the maximum power achieved from our coupled cavity array laser with only ~ 10 nanocavities ($>12 \mu\text{W}$) is about 100 times larger than a single cavity laser (Fig. 4).

Table1. Averaged values of the measured thresholds and DQEs of several single cavity and coupled cavity lasers and their ratios. Also shown are the β -factor ranges obtained by fitting laser rate equations to the measured LL-curves.

	Threshold [mW]	DQE	β -factor
Single Cavity	0.26	0.51	[0.09-0.15]
Coupled Cavity Array	2.68	10.37	[0.03-0.09]
RATIO	~ 10	~ 20	

In our optically pumped lasers, the improvement of DQE can result from two effects: more effective pumping scheme (i.e., an increase in V_{mode}/V_a), and cavity effects (i.e., reduction of $\tau_{\text{mirror}}\Gamma G(N_{\text{th}})$), as explained in Section 2. In our experiment, we know that the pumped active region V_a is approximately ~ 9 -10 times larger with respect to single cavity laser, but we do not know the exact increase in V_{mode} , since some of the 81 cavities in the area may be uncoupled from the lasing mode. Fig. 5 shows the output power from the coupled PC array laser and a single cavity laser, theoretically analyzed by solving rate equations with parameters corresponding to our experimental conditions (Table 2). Clearly DQE increases with the number of coupled cavities (n_c) that are lasing together ($V_{\text{mode,array}}=n_c V_{\text{mode,single}}$). On the other hand, the threshold does not change with n_c , as it is primarily determined by the pumped active volume V_a as explained above. By comparing theoretical analysis shown in Fig. 5 with our experimental results shown in Fig. 4, we conclude that majority of 81 cavities in the array are lasing together in our laser. With such a large number of coupled cavities, the coupled cavity band forms, the lasing occurs from the high symmetry point (Γ), and the individual cavity resonances are not visible as in the case of a small number of coupled resonators [26-17].

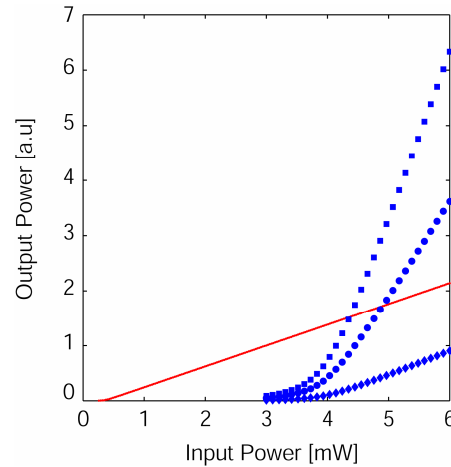


Fig. 5 Output power as a function of the input pump power and the number of coupled cavities in the array, analyzed using rate equations and our experimental conditions (parameters given in Table 2). Single cavity results are shown in red and coupled cavity array laser results in blue. Coupled cavity laser has 10 times larger V_a than single cavity laser, while the mode volume V_{mode} increases relative to that of a single cavity laser by a factor of 10 (diamond), 40 (circle) and 70 (square). By comparing theoretical analysis shown here with our experimental results shown in Fig. 4, we conclude that majority of 81 PC cavities in the array are lasing together in our laser.

4. Conclusion

In summary, we have shown that by ultra-dense coupling of photonic crystal nanocavity lasers with large spontaneous emission coupling factor β , the differential quantum efficiencies can be improved dramatically, without sacrificing the low lasing thresholds of single PC nanocavity lasers. This could not have been achieved by coupling lasers with small β (such as VCSELs). We have experimentally demonstrated coupling of a large number of PC nanocavities ($\beta \sim 0.1$) in a controlled manner, we have also shown that with an increase in the number of coupled cavities, the increase in DQE is significantly larger than an increase in the lasing threshold (with respect to single cavity lasers). We measured peak output powers from the PC laser array that are more than two orders of magnitude higher than in single PC cavity

laser [7]. Furthermore, output powers comparable to conventional single mode VCSELs, but at much lower threshold pump powers, can be achieved by coupling even larger numbers of PC cavities. We expect that such structures can also be directly modulated at high speeds, as a result of a strong localization of light [9], implying that coupled nanocavity arrays can be an effective way to achieve high power and high-speed single mode laser sources.

Acknowledgements

This work has been supported by the MARCO Interconnect Focus Center and in part by NSF ECS-04-24080. The authors would like to thank Dr. Jim McVittie and Mehmet Fatih Yanik for their help in fabrication and Prof. M. Marty Fejer and Prof. David Miller for useful discussions.

A. Laser Rate Equations

The dynamics of carrier density N and photon density P in a laser are given by the following rate equations:

$$\frac{dN}{dt} = \eta \frac{L_{in}}{\hbar \omega_p V_a} - \left(\frac{N}{\tau_r} + \frac{N}{\tau_{nr}} \right) - \Gamma G(N) P \quad (4)$$

$$\frac{dP}{dt} = \Gamma G(N) P + \beta \frac{N}{\tau_r} - \frac{P}{\tau_p} \quad (5)$$

Table 2. Typical parameters for InGaAsP-InP MQWs that are used in solving rate equation.

Surface recombination velocity (V_s) = 10^4 cm/s
Bimolecular recombination coefficient (B) = 1.6×10^{-10} cm ³ /s
Auger nonradiative recombination rate (C) = 5×10^{-29} cm ⁶ /s
Transparency carrier density (N_{tr}) = 1.5×10^{18} cm ⁻³
Gain coefficient (G_0) = 1500 cm ⁻¹
Absorption ration of pump in QW region (η) = 0.26
Confinement factor (Γ) = 0.159
Propagation distance for surface recombination (d_a) = 2×10^{-5} cm
Pumped active volume (V_a) = 2.2×10^{-13} cm ³
Optical mode volume for single cavity (V_{mode}) = 6×10^{-14} cm ³
Lasing wavelength (λ_l) = 1.53×10^{-4} cm
Pump laser wavelength (λ_p) = 0.83×10^{-4} cm

The parameter definition and their values are listed in Table 2. In (4) the carrier density increases with the pump rate (1st term), decreases by radiative recombination (2nd term), non-radiative recombination (3rd term) and stimulated emission (4th term). In the analysis the radiative recombination rate is expressed as $1/\tau_r = BN$. It should be noted that this expression is correct for bulk materials but is not exact for nanocavities since it does not include modification of radiative lifetime in the cavity. For non-radiative processes only surface recombination ($1/\tau_s = V_s/d_a$) and Auger recombination ($1/\tau_A = CN^2$) are included. In (5) the photon density increases with the stimulated emission (1st term) and spontaneous emission that is coupled to the particular lasing mode (2nd term) and decreases with a leakage rate through the cavity by $1/\tau_p$ (3rd term). Following references [22,25], we have assumed in our analysis that the gain is expressed as $G(N) = G_0 c/n_{eq} \log(N/N_{tr})$, with effective index n_{eq} for

our structure. The carrier and photon density is calculated at steady state condition by using (4) and (5). The carrier and photon numbers are given by NV_a and PV_{mode} respectively. The output power is calculated as $L_{out} = \hbar\omega_l PV_{mode} / \tau_{mirror}$. In the analysis we have assumed that $\tau_{mirror} = \tau_p$.